ADVANCED OPTICAL MATERIALS
www.advopticalmat.de

One-Step Formation of Hybrid Nanocrystal Gels: Deposition of Metal Domains on CdSe/CdS Nanorod and Nanoplatelet Networks

*Dániel Zámbó, Anja Schlosser, Rebecca T. Graf, Pascal Rusch, Patrick A. Kißling, Armin Feldhoff, and Nadja C. Bigall**

Hybrid semiconductor-based nanocrystals (NCs) are generally synthesized in organic media prior to their assembly into catalytically promising nanostructures via multistep methods. Here, a tunable, easy-to-adapt and versatile approach for the preparation of hybrid nanoparticle networks from aqueous nanocrystal solutions is demonstrated. The networks consist of interconnected semiconductor NC backbones (made of CdSe/CdS dot-in-rods or core/crown nanoplatelets) decorated with noble metal (Au and Pt) or with metal-based domains (Co^{2+} and Ni^{2+}) demonstrating a powerful synthetic control over a variety of hybrid nanostructures. The deposition of the domains and the formation of the network take place simultaneously (one-step method) at room temperature in dark conditions without any external trigger. Beside the in-depth structural characterization of the gel-like hybrid networks, the wavelength-dependent optical features are studied to reveal an efficient charge carrier separation in the systems and a controllable extent of fluorescence quenching through the domain sizes. Photoluminescence quantum yields and decay dynamics highlight the importance of fine-tuning the conduction band/Fermi level offset between the semiconductors and the various deposited metals playing central role in the electron–hole separation processes. This procedure provides a novel platform toward the preparation of photo(electro)catalytically promising hybrid nanostructures (acetogels and xerogels) without the need of presynthetic hybrid particle design.

1. Introduction

Semiconductor hetero-nanoparticles with tailored and designed electronic structure revolutionized the field of optoelectronics and photovoltaics due to their size-, shape-, and composition-dependent physicochemical properties.[1] Their great applicational potential in optics, electronics, energy harvesting and catalysis lie on the fact, that the formation of a heterojunction in semiconductor NCs (e.g., core/shell or core/crown) can further enhance the fluorescence quantum yield and photostability,[2,3] and additionally, it alters the photoluminescence dynamics of the resulting particles by opening new radiative/nonradiative pathways.[4] Furthermore, anisotropy supports the spatial and thus the temporal separation of charge carriers generated via an incoming photon, which makes these NCs efficient photocatalysts.[5,6] Anisotropy as well as the accessibility of NC surfaces can apparently be further increased via assembling hetero-nanocrystals into porous gel-like 3D macroscopic structures with extended application potential in cases, where the powder- or solution-based NC catalysts suffer from drawbacks (agglomeration and extraction). As we have shown through numerous different gelation techniques recently, the assembly of these NCs provides a platform toward novel fluorescent superstructures with exceptionally high specific surface area, low density and promising (electro) catalytic performance.[7–12] Conduction band offset in CdSe/CdS heterojunction indicates the formation of quasi-type II structure, in which the hole is confined in the core and the electron can delocalize in the shell.[13] While this is valid for nanorods, core/crown nanoplatelets (NPLs) show type I band alignment despite the same heterojunction. This behavior can be attributed to the high exciton binding energy emerging in NPLs: the hole drags the electron to the core, where they recombine radiatively.[14,15]

In quasi-type II and type I cadmium chalcogenide NCs, band-alignment governed interfacial electron transfer (being responsible for outstanding optical properties and catalytic performance) could be further improved by depositing metal domains on the surface of the hetero-nanocrystals.[16,17] Nowadays, the library of the evolving hybrid NCs consists of

Dr. D. Zámbó, A. Schlosser, R. T. Graf, P. Rusch, P. A. Kißling, Prof. A. Feldhoff, Prof. N. C. Bigall
Leibniz Universität Hannover
Institute of Physical Chemistry and Electrochemistry
Callinstr. 3A, 30167 Hanover, Germany
E-mail: nadja.bigall@pci.uni.hannover.de
Prof. N. C. Bigall
Cluster of Excellence PhoenixD (Photonics, Optics and Engineering—Innovation Across Disciplines)
Leibniz Universität Hannover
30167 Hanover, Germany
The ORCID identification number(s) for the author(s) of this article can be found under https://doi.org/10.1002/adom.202100291.

DOI: 10.1002/adom.202100291

numerous combinations of semiconductor NCs and the selectively grown metal domains.

Decorating CdSe/CdS hetero-nanocrystals with catalytically active domains opens up various new routes toward novel, effective and tunable photocatalysts and electrocatalysts. In the recent two decades, control over the synthesis procedures and the understanding of charge carrier dynamics (thus, the catalytic behavior as well) in such systems attracted a paramount research interest. As a result, CdTe quantum dots (QDs), CdSe QDs, CdSe nanorods (NRs), CdS NRs and CdSe/CdS dot-in-rod NCs can be efficiently decorated with Ag,[18] Au,[19–23] Pt,[24–26] AuPd,[27] Ni,[28,29] Co[30–33], $Ni(OH)_2$,[34–36] or $Co(OH)_2$[37] domains; furthermore, we also published a method for the site-selective growth of noble metals on CdSe/CdS core/crown NPLs.[38] The electronic structure of these hybrid NCs (i.e., band alignment, Fermi level) allows the enhancement of the light-induced charge carrier separation endowing them with high potential in photocatalytic applications such as water splitting[16,29,33,35,37–40] or H_2O_2 production.[40,41] Except solely few examples, the abovementioned synthetic procedures take place in organic solvents and require external trigger to initiate the reduction of the metal precursors. This stimulus can be heat, light or the presence of reducing agents. However, if the advantages both of hybrid NCs and their assembly into gel-like structures are aimed to be exploited, a complex multistep organic synthesis and assembling approach must be applied. This approach is time consuming and suffers from the drawbacks of the often poor stability of hybrid NCs in solution. Hence, to date, the number of studies dealing with one-step formation of hybrid semiconductor–metal NC superstructures is limited, and the most important study is restricted to CdSe nanorods with Pt.[42] Although, selective growth of Au on CdSe/CdS NRs in aqueous phase has been achieved experimentally (without assembling them), the procedure requires UV illumination as well as a reducing agent.[43]

Therefore, we aimed to establish a novel strategy to prepare hybrid NC gel networks, where the advantageous properties at the NC level as well as at the micro- and macrostructural level can be utilized via the controlled assembly of tailored semiconductor NCs (decorated with metal domains) into NC gels directly from aqueous phase. Our recent study demonstrated, that CdSe/CdS dot-in-rods and core-crown NPLs with different surface chemistry are able to be assembled into porous gel structures via addition of inert trivalent cations at room temperature.[8] The question arose, whether the assembly and the deposition of catalytically active domains might be achieved in a single step method without external stimuli, through applying highly reactive metal salts.

In this paper, we demonstrate a novel method for the one-step preparation of porous, hyperbranched hybrid semiconductor–metal gel structures, with control over the structural and optical properties. Using two types of nanocrystals as backbones (CdSe/CdS dot-in-rods and core/crown NPLs) with different thiolated ligands, this platform provides interconnected nanocrystal networks containing catalytically active domains evenly distributed throughout the entire network with preserved initial particle morphology. This versatile approach allows the deposition of different noble metal (Au and Pt) and metal-hydroxide ($Ni(OH)_2$ and $Co(OH)_2$) domains onto the semiconductor backbone providing significantly enhanced charge carrier separation upon illumination. The key advantage of our technique lies in its one-step nature: the formation of the semiconductor backbone and the deposition of the catalytically active domains take place simultaneously without external trigger (light, heat, and reducing agent). Consequently, the domain formation does not require heat, illumination, or additional reducing agents, which makes this process easy-to-adapt and versatile. This work aims to break the paradigm, that the decoration of the building blocks (generally in organic phase) must be performed prior to the assembly. Due to the interconnection of the decorated semiconductor NCs, the charge carrier mobility is further enhanced, as a result, these hybrid nanostructures have great application potential as photo(electro)catalysts.

2. Experimental Section

As backbones of the hybrid nanocrystal gel networks, CdSe/CdS dot-in-rods and core/crown nanoplatelets were chosen. The particles were synthesized via the hot injection method based on the procedures published elsewhere for NRs[44] and NPLs[15,45] with applied improvements (see the Supporting Information for the detailed description). Prior to the assembly, the nanocrystals were transferred from organic to aqueous phase using mercaptopropionic acid (MPA) for NRs and mercaptoundecanoic acid (MUA) for NPLs according to the previously published protocol.[46] Phase transfer is of essential importance before triggering the assembly: it provides a covalently bound, hydrophilic ligand shell around the NCs that helps to control the kinetics of the assembly process through the modulation of the interparticle forces (electrostatic and steric interactions). According to experience, MUA provides enhanced stability and helps retain the photoluminescence quantum yield of NPLs compared to MPA. It has to be noted, that due to the more prominent degree of passivation of the CdSe core, phase transfer leads to less loss of quantum yield (QY) for dot-in-rods compared to core/crown NPLs. Nevertheless, after phase transfer, both colloidal systems have excellent stability (over 6 months), retained particle morphology and remarkable fluorescence. The previous studies revealed the optimal concentration of CdSe/CdS nanocrystals for gelation,[7,8] thus, the Cd concentration of the aqueous NC solutions was set to 3.6 g L^{-1} (equals to 32×10^{-3} M, measured by atomic absorption spectroscopy, AAS) in both solutions and this concentration was applied for all further experiments. Afterward, the aqueous NC solutions were introduced into Eppendorf tubes followed by the addition of the aqueous Au^{3+}, Pt^{4+}, Ni^{2+}, or Co^{2+} salt solutions in different concentrations keeping the final NC concentration constant (see the Supporting Information for experimental details). The mixtures were vortexed immediately for 2 s, then were kept in a dark place free of vibration for 17 h (overnight). After the network formation occurred, the Eppendorf tubes were filled with MilliQ water well-above the hydrogels as a first step of the gel washing procedure. The hydrogels were washed thoroughly in multiple steps with MilliQ water followed by the gradual change of the medium to anhydrous (extra dry) acetone through different H_2O:acetone solvent mixtures. The preparation of the final acetogels is time-consuming; however, this time period also involves the necessary aging of the gel structure and

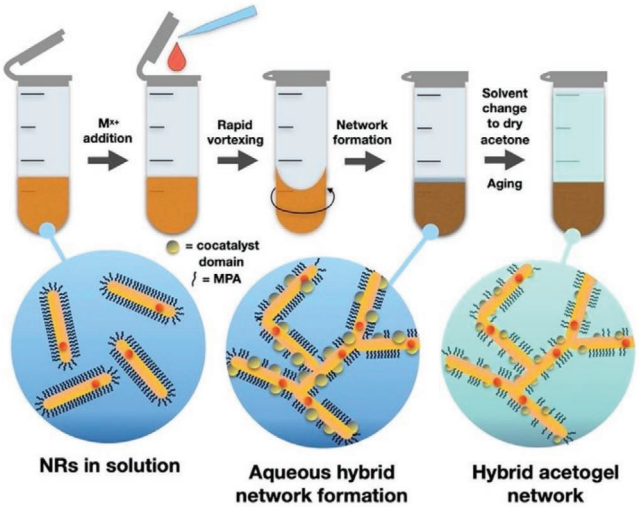

Scheme 1. Schematics of the preparation of hybrid nanoparticle gel networks from aqueous colloidal nanocrystal solution illustrated through the example of CdSe/CdS dot-in-rods.

ensures the removal of the excess of cations, detached ligands, water and provides extremely clean hybrid nanocrystal gel networks that are stable over time and free of byproducts. Additionally, anhydrous acetone as the medium of the gels allows the preparation of TEM and SEM samples with conserved gel morphology due to the significantly reduced capillary forces upon rapid drying.[7,8,47] As a further advantage, acetogels can be potentially dried supercritically, opening up new routes toward hybrid NC aerogels in the future.[7,8] **Scheme 1** summarizes the steps of hybrid acetogel preparation detailed above.

Micro- and nanostructural properties, elemental composition, and crystallinity of the prepared hybrid acetogel structures were revealed by scanning electron microscopy (SEM), transmission electron microscopy (TEM), energy-dispersive X-ray spectroscopy (EDX), and X-ray diffraction (XRD) via drop-casting fragments of the gel (diluted with anhydrous acetone) onto Si wafers or Cu grids. For the optical measurements, the gels were transferred into quartz cuvettes. For all samples, extinction, UV–vis absorption and emission spectra, as well as PL lifetimes and quantum yields have been determined at different metal ion concentrations (latter ones only where detectable emission was observed). For detailed experimental descriptions of materials, synthetic routes and characterization methods please refer to the Supporting Information.

3. Results and Discussion

3.1. Structural Properties of Hybrid Nanostructures

Assembling nanocrystal solutions always requires the synthesis of high quality and deeply characterized building blocks. As the first step, CdSe/CdS dot-in-rod nanoparticles and core/crown NPLs were synthesized and phase transferred followed by the in-depth optical and structural characterization. The dimensions of the NRs were found to be 40.3 (±2.6) nm × 5.7 (±0.2) nm, while the NPLs have dimensions of 17.5 (±2.5) nm × 23.1 (±2.9) nm. Representative TEM images and the optical properties of the initial nanocrystals are presented in Figures S1 and S2 (Supporting Information) for NRs and NPLs, respectively. Network formation as well as metal deposition were triggered by the addition of Au^{3+}, Pt^{4+}, Ni^{2+}, and Co^{2+} aqueous solutions (prepared from the respective metal chloride salts) in different concentrations to optimize the gelation process and to reveal the concentration-dependent optical properties of the assemblies.

During the optimization process, the formation of macroscopic, homogenous gels with minimal shrinkage (compared to the initial NC solution) was targeted. For NRs, 1, 5, and 10×10^{-3} M of salt solutions were added, however, in case of 1×10^{-3} M, observable gelation did not occur. In contrast, applying 5×10^{-3} or 10×10^{-3} M salt solutions, hydrogels with negligible shrinkage could be obtained (Figures S3 and S4, Supporting Information) proving the formation of porous, voluminous, branched nanocrystal networks.[8] **Figure 1** shows the structure of hybrid acetogels built up from NRs applying 10×10^{-3} M metal salt solutions (TEM images of the networks prepared via 5×10^{-3} M metal salts can be seen in Figure S5 in the Supporting Information).

Based on these results, NPLs were also assembled using 10×10^{-3} and 18×10^{-3} M metal salts: MUA on the NPLs surface increases their stability against multivalent cations;[8] hence, higher concentrations are needed to be applied leading to similarly decorated networks as for NRs (**Figure 2**). For both NR and NPL backbones, addition of metal cations led to hyperbranched, interconnected hybrid nanocrystal networks, where the NCs are mainly tip-to-tip (for NRs) or edge-to-edge (for NPLs) assembled and evenly decorated with domains. For Au and Pt, the size of the noble metal domains was found to be tunable through the concentration of the added metal salts (Figure 1A,B compared to Figure S5A,B in the Supporting Information and Figure 2A,B to Figure S6A,B in the Supporting Information), while an increasing concentration of Ni^{2+} and Co^{2+} led to structures possessing domains with similar sizes. This observation was also supported by elemental composition analysis (SEM-EDX), that shows increasing Au and Pt content but solely moderate increase of Ni and Co content in case of higher metal salt concentrations for NRs and NPLs as well (Figures S7 and S8, Supporting Information).

Similar to the mechanism of ionic gelation of CdSe/CdS NRs and NPLs we published recently,[8] it can be assumed that multivalent cations facilitate the replacement as well as the cross-linking of the surface grafted thiol-terminated carboxylic acids (MPA). It can be hypothesized that the applied high valence metal cations replace the cadmium-thiolates on the NC surface as Z-type ligands. However, due to the occupied d-orbitals of the applied noble metal cations, this replacement likely takes place only after a complexation of the cations via, e.g., free ligands, which allows the ligand replacement in the next step and facilitates the controlled destabilization of the aqueous NC solutions resulting the mainly tip-to-tip (for NRs) and edge-to-edge (for NPLs) connected nanoparticle backbone. In this work, we also used multivalent cations to trigger the network formation, however, these are highly reactive metal salts which tend to nucleate heterogeneously. Therefore, not solely the network forms (due to the destabilizing effect of these multivalent metal salts), but the formation of metal-containing domains also takes

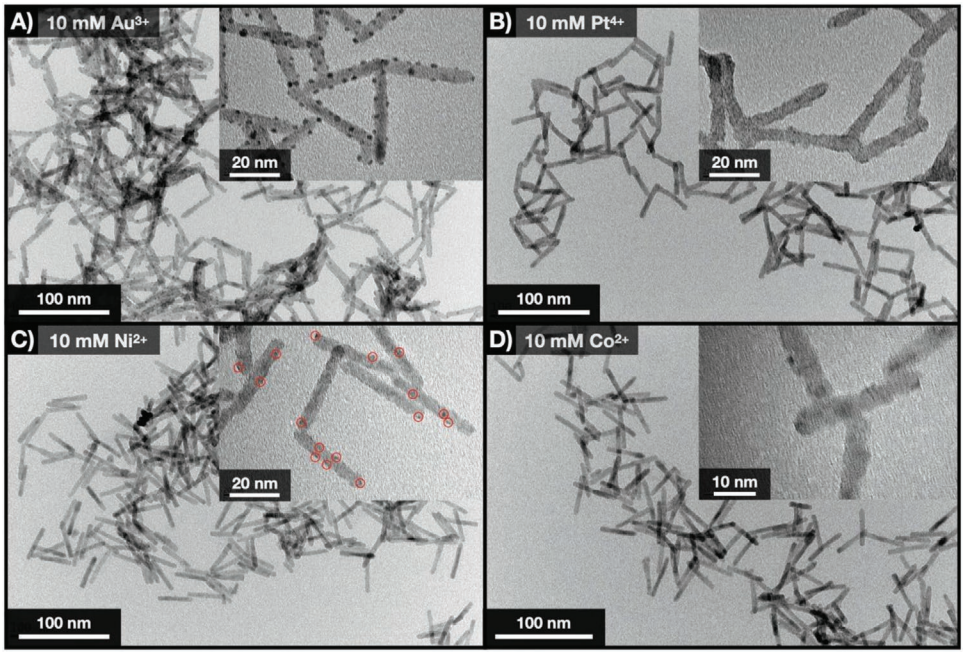

Figure 1. TEM images representing the structure of the hyperbranched interconnected semiconductor NR backbone prepared with 10×10^{-3} M Au^{3+}(A), Pt^{4+}(B), Ni^{2+}(C), and Co^{2+}(D). The insets show the NRs decorated with domains at higher magnifications. Due to the low visibility of the Ni-containing domains, red circles are guide to eye in panel (C). All samples were prepared from acetogels.

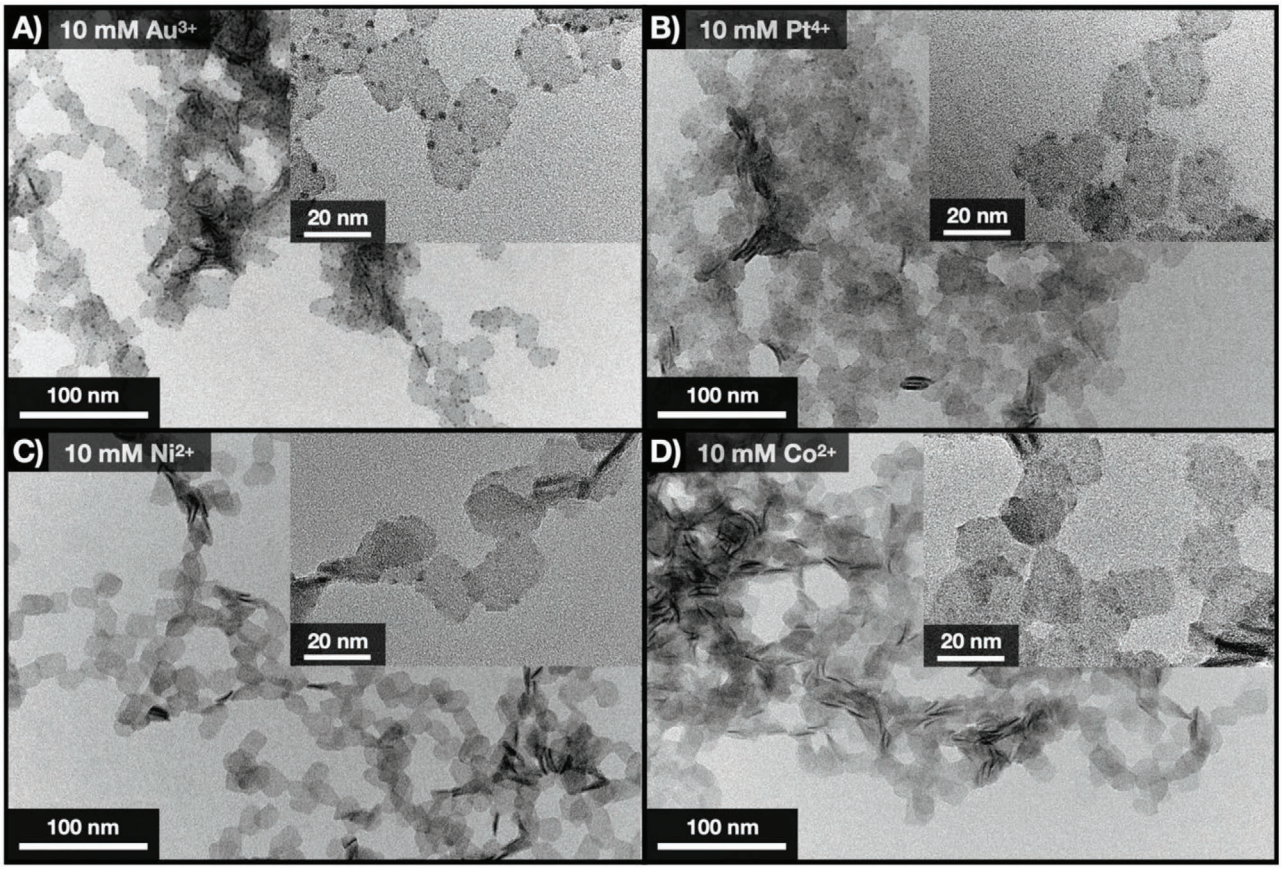

Figure 2. TEM images representing the structure of the hyperbranched interconnected semiconductor NPL backbone gelated via Au^{3+} (10×10^{-3} M, A), Pt^{4+} (10×10^{-3} M, B), Ni^{2+} (10×10^{-3} M, C), and Co^{2+} (10×10^{-3} M, D). The insets show the (co)catalyst domains at higher magnifications. All samples were prepared from acetogels.

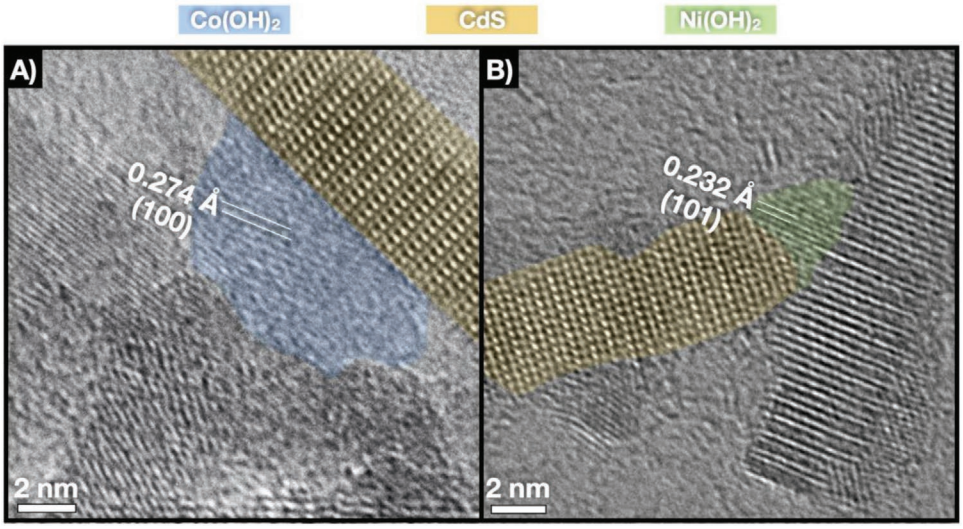

Figure 3. HR-TEM images of hybrid NR gel networks prepared via 10×10^{-3} M Co^{2+}(A) and 10×10^{-3} M Ni^{2+}(B) cations representing the presence of $Co(OH)_2$ and $Ni(OH)_2$ domains.

place. In contrast to the observations of Elmalem et al.[42] (dissolution of CdSe upon Pt deposition), our semiconductor NCs preserve their size upon gelation and decoration (Figure S9 in the Supporting Information demonstrates that neither the length nor the width of the NRs changes after the decoration with larger Au domains using 10×10^{-3} M Au^{3+} ions). Based on this finding, the initial nucleation of the domains is likely assisted by the defect sites on the CdS shell (or crown) and by the surface-grafted thiols acting as reducing agents. These processes make the heterogeneous nucleation of the metals more favorable compared to the homogenous metal NP formation in the solution, thus, the decoration of the backbone occurs.

For hybrid NR gels, the deposited domains do not show preferences regarding their spatial location around the rods: the domains are equally and evenly distributed in the interconnected nanorod networks. Due to the domain formation on the tip region of the rods as well, in some cases, the interconnecting area between rods consists of CdS-CdS as well as domain-CdS connected regions simultaneously (comparative HRTEM images on NR–NR connections are shown in Figure S10 in the Supporting Information). In contrast, platinum shows island-like growth around the nanorods;[48] however, these islands also have distinct borders (inset of Figure 1B). Based on the TEM images, the growth of domains containing Ni^{2+} and Co^{2+} looks similar to gold (i.e., distinct, quasispherical domains are formed), however, their low electron contrast makes the imaging cumbersome. Instead, domains in hybrid NPL assemblies nucleate and grow on the edge region of the NPLs more preferably, that agrees well with our observations in solution-based NPL-Pt systems.[38] Nevertheless, this does not hinder the formation of direct NPL-NPL connections and all types of domains show distinct, quasispherical shape (comparative HRTEM images on NPL-NPL connections are shown in Figure S11 in the Supporting Information).

For noble metal domains with higher atomic numbers, the deposited materials can be visualized in a straightforward manner, however, in case of Ni^{2+}- and Co^{2+}-gelated structures, due to the low electron contrast and crystallinity of the domains, other techniques had to be applied. HRTEM and STEM images of hybrid NR@Co and NRs@Ni structures show, that although the domains accumulate in certain areas on the NR's surface, a thin continuous layer is formed around the rods (Figure S12, Supporting Information). In the domains, *d*-spacings of the lattices agree well with the value of $Co(OH)_2$ (0.274 Å for {100} facet) and $Ni(OH)_2$ (0.232 Å for {101} facet) in the respective systems as **Figure 3** shows.

Spatial distribution of the deposited domains was further analyzed for the Co^{2+}-gelated NR network. EDX elemental maps reveals quasiequivalent loads of domains on the connected NRs and NPLs upon gelation via Co^{2+} and Ni^{2+} (Figure S13, Supporting Information). To further prove, that the domain deposits as a thin layer on the surface of the NRs, electron energy loss (EEL) spectra were taken from a region of interconnected NRs (**Figure 4**A,B). Spatially resolved EEL spectra show (Figure 4C–E), that the Co-containing domain is present on the NRs surface relatively evenly (the Co-L_3 and Co-L_2 white lines appear in the region where NRs are also present). These observations underline the major difference between the formation of the domains for noble metal and metal-assisted assembly: Au and Pt nucleates forming more distinct domains, while connected building blocks formed via Ni^{2+} and Co^{2+} are covered by the deposited domains as a layer.

EELS also shows the presence of oxygen (O-K ionization edge) in the sample; however, the origin of the oxygen can be bifold: i) MPA molecules on the NR surface contain oxygen due to their $-COO^-$ groups and ii) the deposited domain consists of Co and O. The former would lead to weaker O signal in EELS if we assume only the presence of residual MPA molecules on the NR surfaces. Additionally, O-K ionization edge becomes more prominent if Co also appears on the respective measurement spot. Consequently, the domains contain Co and excessive O beyond the O content of the ligands. Based on the fact, that the Co^{2+} cations are added to aqueous NC solutions at alkaline pH, the formation of $Co(OH)_2$ is the most favorable reaction.

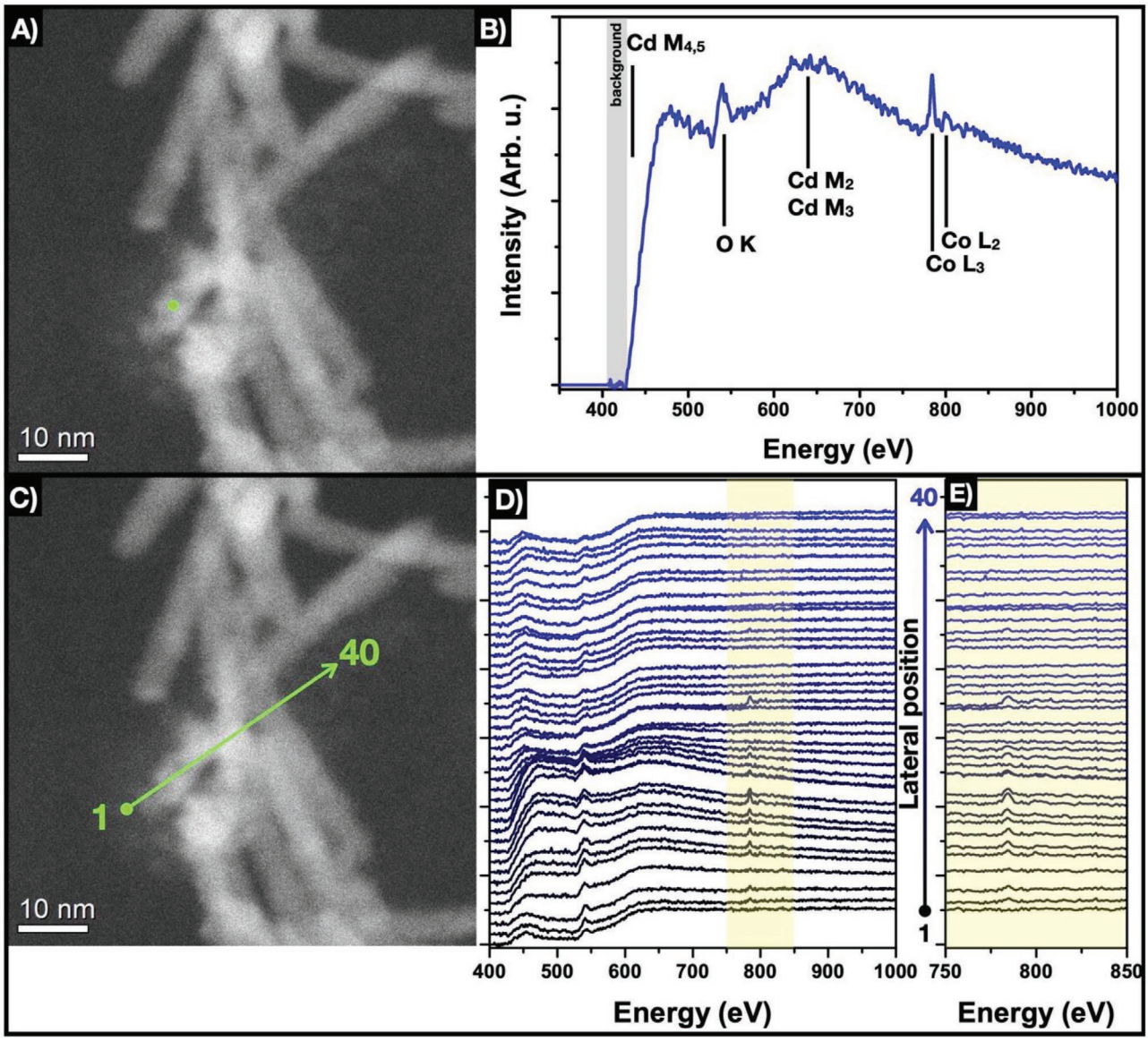

Figure 4. STEM images A,C) and EELS analysis B,D,E) of hybrid NR gel networks prepared via 10×10^{-3} M Co^{2+} cations. A representative EEL spectrum (B) was collected from the green spot marked in panel (A). EELS line scan (D) was recorded along the green arrow (equals to 36 nm in length, 40 spectra) in panel (C). Panel (E) shows the EEL spectra in the energy window relevant for Co.

XRD results show changed peak ratios upon gelation along with a slight shift (compared to the pristine NRs) which can be attributed to the deposition-induced lattice strain effect between the CdS and the deposited hydroxides[49] and indicates, that the domains mostly form on the {100} and {101} facets of the shell (Figure S14, Supporting Information). Nevertheless, reflections from any relevant Co- or Ni-containing hydroxides, oxides or oxyhydroxides are not able to be detected. This can be attributed to the relatively low amount and low crystallinity of the domains on the NCs surface, as other studies have also shown.[35,37,50–52] It is important to emphasize, that the formation of cobalt oxides and nickel oxides (as well as oxyhydroxides) can only be possible at elevated temperatures,[53,54] thus, the presence of these materials can be ruled out. The experimental conditions and the observed structural properties of the domains agree well with the theory of $Co(OH)_2$ and $Ni(OH)_2$ formation. As the structural and compositional properties indicate, the Ni^{2+}- and Co^{2+}-gelated hybrid structures differ from the ones generated via the addition of noble metal cations. This can be attributed to i) the less reactivity of the Ni^{2+} and Co^{2+} cations (forming Ni^0 and Co^0 only via pyrolysis[55] or in the presence of hydrazine/polyols)[56,57] and ii) to the favorable formation of stable hydroxides in the presence of OH^- ions. The formation of the metal hydroxide domains is a precipitation-driven process;[34,50,52] thus, the excess surface energy of the semiconductor NPs might play an important role in the deposition of the hydroxides on the NRs and NPLs. The nucleating domains destabilize the NCs upon growing further facilitating their interconnection.

Interestingly, we observed an increasing electron contrast of the Co- and Ni-containing domains in case of longer exposure

to the electron beam in the TEM (Figure S15, Supporting Information), indicating the formation of metallic Co and Ni under these conditions. This implies the reduction of Co^{2+} and Ni^{2+} cations from the $Co(OH)_2$ and $Ni(OH)_2$ domains to Co and Ni upon irradiation with electrons. Similar electron excess (due to charge carrier separation, explained below) can be evolved in the hybrid nanostructures in photo(electro)chemical processes upon irradiation with photons, that makes the initial domains potential sources to form metallic domains in situ, which can be utilized in electrochemical processes.[34,35,52] The in situ formation of the metallic domains can be supported by scavenging the holes via the OH^- anions[58] or the surface attached thiolated ligands on the surface of the NCs.[59]

3.2. Optical Properties and the Mechanism behind Them

Depositing noble metal or metal domains on the surface of semiconductor nanoparticles might lead to a partial or complete quenching of the initial photoluminescence, which highly depends on the size and number of the domains (i.e., metal or metal-hydroxide load).[39,60] Additionally, in hetero-nanoparticle systems, the wavelength of irradiation also alters the optical processes depending on the nanoscale component being irradiated (core and/or shell/crown). To overhaul the effect of the excitation wavelength, all optical measurements were carried out from 350 to 550 nm (for NRs) and from 350 to 515 nm (for NPLs) in distinct steps. This allows to understand the radiative processes upon generating excitons in the hetero-nanoparticles. In perfect agreement with Hinsch et al.,[61] the QY of the pure NRs shows dependency on the excitation wavelength (Figure S1C, Supporting Information): exciting the CdSe core ($\lambda_{exc} \geq 500$ nm) leads to significantly higher QYs due to the better passivation of the core embedded in the CdS shell.[62] For core/crown NPLs, the above discussed change of QY is much less remarkable (manifesting itself in only an increase of 0.54%; see Figure S2B in the Supporting Information) that can be attributed to the much less passivated CdSe core and the much higher volume ratio between CdSe and CdS (compared to the NRs).

Due to the small domain sizes in the hybrid NRs assembled via 5×10^{-3} M salts, residual fluorescence can be detected for all NR systems. However, for NPLs, 10×10^{-3} M Au^{3+} salt caused complete quenching and weak, but detectable emission for 10×10^{-3} M Pt^{4+} is observed only by irradiating the CdSe core NPLs, that can be attributed to the smaller size of Pt domains in this particular case. For higher concentrations, noble metals cause complete fluorescence quenching, while Ni^{2+} and Co^{2+} preserves some radiative pathways for both NC systems. Peak positions of the emissions show bathochromic shift compared to the building blocks without changing the FWHM values significantly (**Figure 5**A,C). This bathochromic shift can be attributed to i) the refractive index change in the vicinity of the nanoparticles, that is the superposition of two factors: the change of the solvent (water to acetone) and the growth of the domains on the NCs surface; ii) the reabsorption of the emitted light due to the high nanoparticle concentration in the gel samples. Furthermore, hybrid NPL gels show larger shifts than the NR gels. This difference points out the diversity of the model systems: while the core is embedded into the shell for NRs, core NPLs are more exposed to the changes of the chemical environment (due to the growth of the crown solely along their edges), thus, their emission shows higher sensitivity to the domain formation and solvent replacement.

Extent of quenching was investigated via PLQY measurements on the acetogels. Based on the significant Fermi-level differences of the deposited domains, Pt quenches the most followed by Au, Co and Ni (Figure 5B,D for QY values of NR and NPL systems). It has to be emphasized, that for hybrid NRs networks, the wavelength of excitation has a remarkable effect on the QYs similar to pure, aqueous NRs (Figure S1C, Supporting Information). Irradiating the CdS shell ($\lambda_{exc} \leq 450$ nm) leads to significantly lower QYs compared to wavelengths, where only the CdSe core absorbs ($\lambda_{exc} \geq 500$ nm). Due to the band alignment of the quasi-type II heterojunction, radiative recombination can only occur inside the core. By exciting the core, the probability of the radiative recombination is remarkably higher than by exciting the shell, which is decorated with the domains facilitating the charge carrier separation. In case of NPLs, this trend is much less obvious due to the above-mentioned differences in the passivation of the CdSe core as well as the CdSe:CdS volume ratio. Additionally, core NPLs might also be partly decorated with domains that hinder the radiative pathways inside the core.

Photoluminescence decay dynamics were also measured for the hybrid NR and NPL gel structures in order to reveal the wavelength-dependent lifetimes in the different hybrid gel systems. PL decay curves of the pure NRs and hybrid NR gel structures can be seen in **Figure 6**. Decay curves were measured at three different excitation wavelengths (368 and 454 nm for irradiating the shell, while 572 nm for exciting the core) and evaluated by multiple exponential fitting (bi- and triexponentials). Fitted components and average lifetimes can be found in the Supporting Information (Table S1, Supporting Information). Pure NRs@MPA in water do not show prominent differences in decay dynamics as a function of the wavelength (from 368 to 572 nm, τ_{AV} decreases from 17.8 to 16.1 ns). However, gelation and deposition of the domains magnifies these minor differences significantly. In each system, domain deposition reduces the lifetime of the excitons. Additionally, excitation at the core wavelength leads to even shorter exciton lifetimes, that agrees well with the observed higher QYs at wavelengths above 500 nm.

The question arises, whether this residual QY and the reduced lifetime can be attributed to inhomogeneous quenching, namely some NRs are not decorated, while others are totally quenched. PL decay components show, that in each system (where fluorescence is detectable), τ_1 and τ_2 are significantly and simultaneously reduced. This implies that the system is homogenously quenched, that is the emission does not originate from NRs (or NPLs) that are not decorated.[32] In case of the presence of bare/undecorated NCs, the PL dynamics should not change while the QY would decrease. Figure 6C,D (and Table S1 in the Supporting Information) shows that increasing amount of Ni^{2+} and Co^{2+} further shortens the PL lifetimes, that suggests a spatially more extended coverage of the connected NRs. Exciting the core QD (at 572 nm), exciton lifetimes become significantly shorter, that implies a faster charge carrier separation in the hybrid hetero-nanoparticle assemblies: electrons can further travel to the domains through

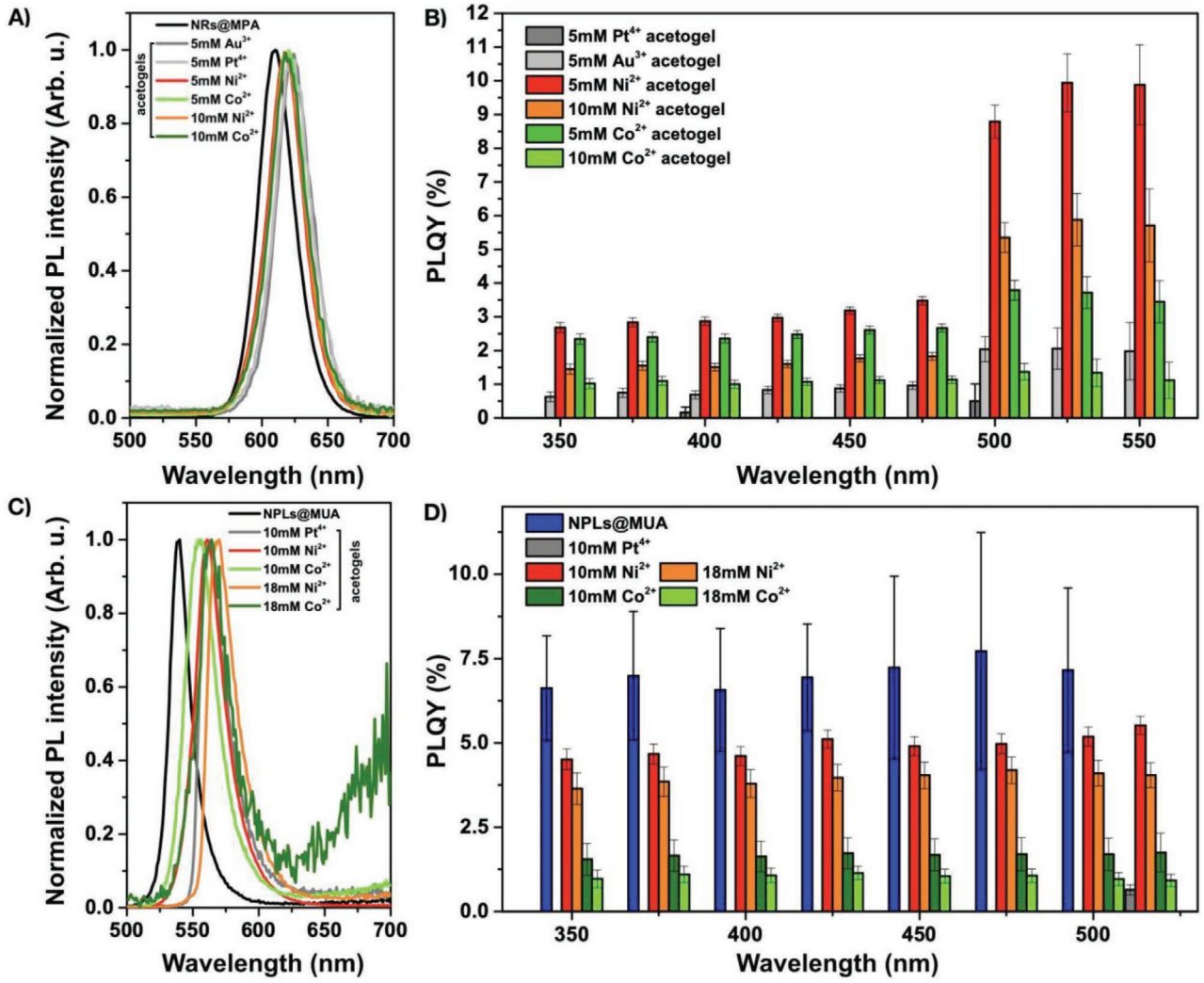

Figure 5. Emission spectra (A,C) and wavelength-dependent PLQY values (B,D) of pristine nanoparticles in solution and hybrid acetogel networks prepared from CdSe/CdS dot-in-rods (A,B) and CdSe/CdS core/crown NPLs (C,D) via metal salt solutions with different concentrations.

the CdS shell; however, this process is more efficient without being surrounded by trap states in the shell region. Based on the structural characterization of hybrid NR gel structures, domains are also present on the rod's surface which is in the vicinity of the core, and thus makes the separation of charge carriers (evolved in the core) faster.

It has to be noted, that gelation itself causes dramatic elongation of the exciton lifetimes in nondecorated NR gel systems[7,8] due to the enhanced electron mobility across the interconnected NRs. This is the reason of the evolution of a third lifetime decay component in the hybrid NR gel structures (even with a τ_3 of up to 67 ns but with low contribution; see Table S1 in the Supporting Information). However, this component becomes less prominent upon irradiation at the core wavelength (572 nm) demonstrating a faster recombination in the vicinity of the core compared to the shell, where the delocalization of the electrons between neighboring NRs might occur.[47]

Decay dynamics shows slightly different behavior for hybrid NPL gels. While gold completely quenches the fluorescence in both applied concentrations, platinum and cobalt initiate similar changes in the lifetime components of NPLs as for NRs: PL lifetimes decrease from 9.5 ns (NPLs@MUA in water) to 3.4 and 5.0 ns for Pt^{4+} and Co^{2+}, respectively (Figure S17 and Table S2, Supporting Information). However, Ni^{2+} facilitates the increase of the average lifetimes even for 10 or 18×10^{-3} M concentrations. This can be attributed to the more prominent contribution of the τ_3 component (see Table S2 in the Supporting Information), which suggests different exciton recombination dynamics in the Ni^{2+}-gelated system.

Optical investigation of the hybrid structures revealed an efficient charge carrier separation in all systems which manifests in significantly suppressed radiative recombination pathways. This effect is the superposition of the hole confinement in the CdSe cores and the presence of the domains acting as electron sinks. This behavior makes these superstructures promising candidates as photocatalysts and photoelectrocatalysts with tailorable composition, material combinations, structural and optical properties.

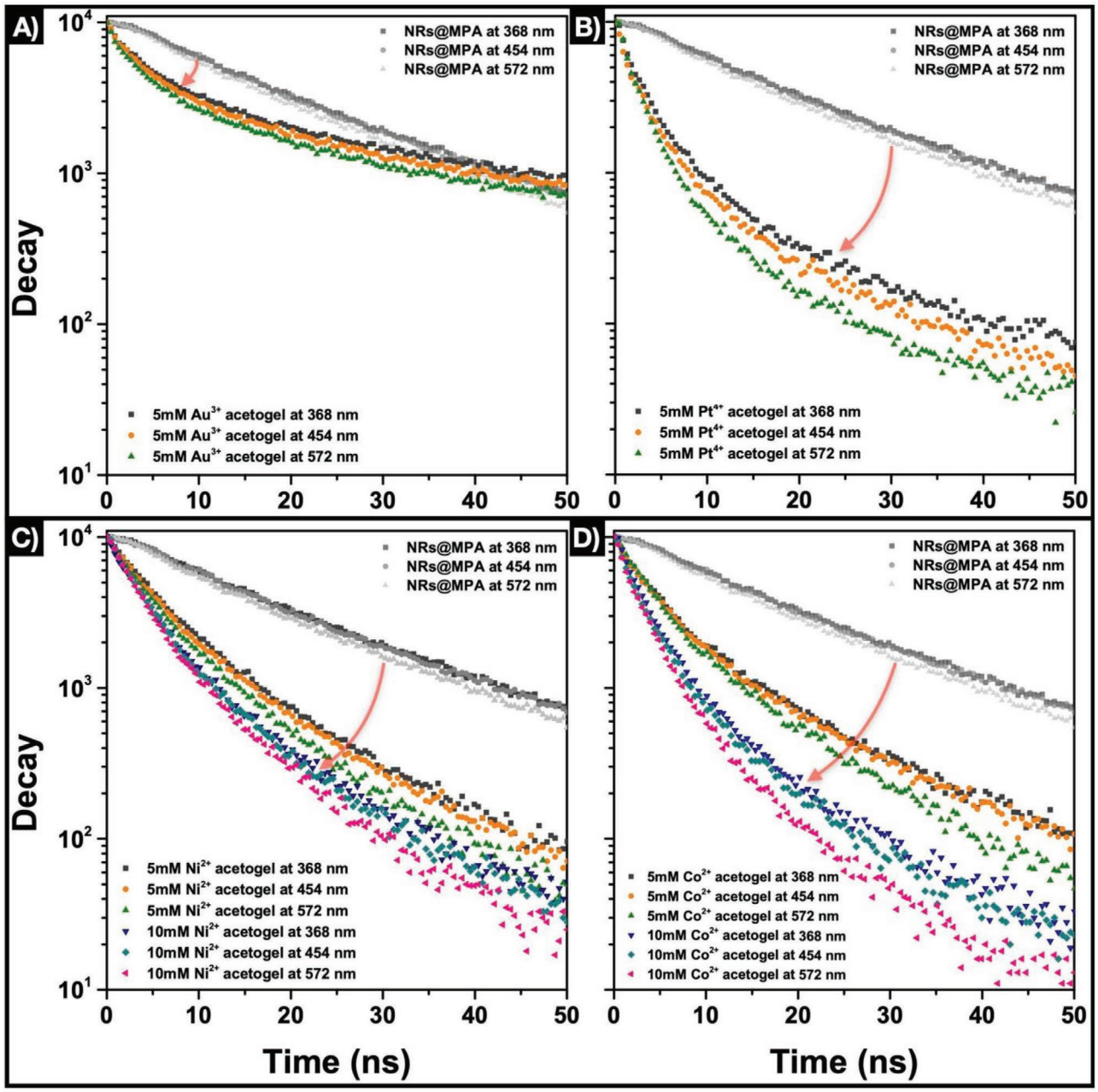

Figure 6. Photoluminescence lifetime decays of different hybrid NR acetogels gelated via Au^{3+} (5×10^{-3} M, A), Pt^{4+} (5×10^{-3} M, B), Ni^{2+} (5 and 10×10^{-3} M, C), and Co^{2+} (5 and 10×10^{-3} M, D) at different excitation wavelengths. The gray scattered curves represent the decay of pristine NRs in solution at different excitation wavelengths. Orange arrows show the trend of the decay changes from pristine NRs to hybrid acetogel networks.

Supported by the above-discussed charge-carrier dynamics, a mechanism is established for NR-based as well as NPL-based hybrid gel structures. **Figure 7** schematically illustrates the pathways of the charge carrier transport in case of two interconnected, decorated NRs. Based on the well-known band alignment of CdSe/CdS heteroparticle system, electrons are able to be delocalized over the CdS shell upon illumination, while the holes are confined in the CdSe core region.[7,8,47] This can be possible due to the slight energy difference between the conduction bands of CdSe and CdS in such dot-in-rod particles. Interconnection between NRs opens up routes toward further delocalization of electrons from one NR to another as our previous experiments[7,8] and calculations[47] have already demonstrated.

Two main pathways can be distinguished, which are shown in Figure 7B,C. Considering an exciton, which is generated in the vicinity of the core, the electron tends to accumulate in the closest domain (while the hole is moving toward the core). However, if the exciton is generated closer to the NR–NR connection, the electron is able to travel through this region and accumulates in the domain of the neighboring rod. This makes the network a continuous semiconductor backbone, where

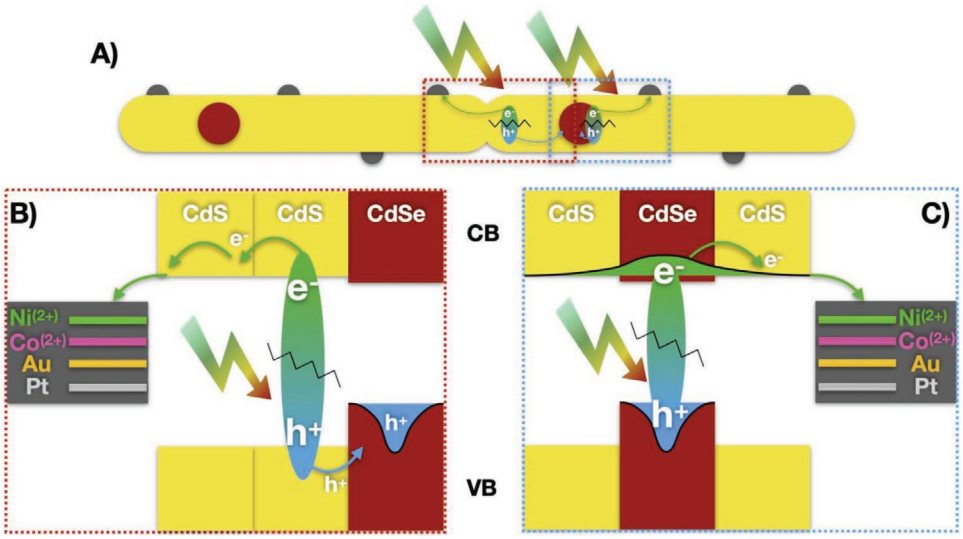

Figure 7. Suggested mechanism of charge carrier transport within the interconnected hybrid NR gel network (A). Detailed illustration of the possible pathways of charge carrier separation closer to the NR–NR interconnected area (B) and in the vicinity of the CdSe core (C). Band alignments interpret the valence band (VB), the conduction band (CB) of the quasi type-II semiconductor NR as well as the Fermi level of the noble metal and in situ generated metal domains. Green and blue arrows indicate the moving direction of the charge carriers (electron: green; hole: blue).

the charge-carrier separation toward the domains can be significantly enhanced based on the possible delocalization of the electrons. The applied metal salts initiate the formation of the domains possessing different Fermi levels. The Fermi level of the domain material alters the extent of fluorescence quenching, and consequently, the efficiency of the electron–hole separation. Based on the relative alignment of the Fermi levels in the prepared hybrid nanostructures,[32,40,63] Pt and Au accumulate electrons more efficiently than in situ generated Co and Ni. This is in agreement with the measured QYs as well as average exciton lifetimes.

The interesting exception from the above discussed trend is the Ni^{2+}-gelated NPL system. Here, an elongation of the exciton lifetime was observed (Figure S17, Supporting Information), that apparently does not fit the explanation given above. However, in case of NPLs, the much more prominent exciton binding energy has to be taken into account in an established mechanism (see Figure S18 in the Supporting Information). While Pt, Au and Co have low enough Fermi levels to facilitate the charge carrier separation, the Fermi level of Ni lies prominently closer to the conduction band of CdSe/CdS. This manifest itself in a significantly smaller driving force toward the accumulation of the electron in the domain, being comparable with the exciton binding energy. Therefore, two driving forces act in parallel: the electron hole-separation via the domain, and the high exciton binding energy. Consequently, the separation of electron and hole becomes less favorable, thus the domain can only delay the recombination of the bound exciton. Considering the fact, that we have not observed electron delocalization in interconnected NPL gel structures so far (likely due to the high exciton binding energies in such systems), the longer PL lifetime in NPL@Ni hybrid structures can be attributed to this slowed down recombination of the exciton in the CdSe core NPL.

In order to expand the range of investigated systems, xerogels were also prepared from the solvogels. Despite the drying at ambient conditions, the structures preserved remarkable porosity for both the hybrid NR (Figures S19 and S20, Supporting Information) and NPL xerogels. PL decay dynamics of xerogels reveals an even more enhanced charge carrier separation (manifesting itself in further reduced PL lifetimes for all systems; Figure S21 in the Supporting Information), which can be attributed to the more NC-NC connections and the denser structures compared to the acetogels. These findings point toward the future application of these hybrid nanostructures, due to the easier handling of xerogels.

4. Conclusions

In summary, a new strategy for the preparation of various hybrid semiconductor–metal and semiconductor–metal hydroxide NC networks was developed. In contrast to the literature methods, our approach does require neither the synthesis of the hybrid NC building blocks prior to their assembly, nor the application of external stimuli (e.g., heat, light illumination, reduction agent). The formation of the interconnected, hyperbranched NC backbones (consisting of connected CdSe/CdS dot-in-rods and core/crown NPLs) and their decoration with domains occur in one single step at room temperature via the addition of aqueous metal cations. These cations act as destabilizing agents as well as precursors for nucleation of the noble metals or metal hydroxides on the NCs. The procedure provides voluminous hybrid NC solvogels, where the synergistic properties of the semiconductor NCs as well as the domains can be utilized. Highly reactive Au^{3+} and Pt^{4+} salts instantly form noble metal domains, while metallic Ni and Co domains can be formed in situ through hydroxides, due to the excited electrons. The structural characterization of the hybrid structures showed that the NRs are mainly tip-to-tip connected, while the NPLs are edge-to-edge connected and the domains are evenly

distributed on the NCs surface. The extent of PL quenching can be tuned by the amount of the added cations (through the size and number of the evolving domains); thus, it was revealed that effective charge carrier separation can be obtained in all synthesized systems. Due to the different Fermi levels of the domains, radiative recombination of charge carrier can be partially preserved, however, the photogenerated electrons have a high affinity to the domains. The structural diversity, the versatility and the demonstrated powerful control over the synthesis of these hybrid NC gel networks make them promising candidates for novel artificial photocatalytic systems toward clean and pure renewable fuels or sensing.

Supporting Information

Supporting Information is available from the Wiley Online Library or from the author.

Acknowledgements

The project leading to these results was funded by the European Research Council (ERC) under the European Union's Horizon 2020 research and innovation program (grant agreement 714429). The authors acknowledge the financial support from the German Federal Ministry of Education and Research (BMBF) within the framework of the program NanoMatFutur, support code 03X5525. In addition, this work was funded by the German Research Foundation (Deutsche Forschungsgemeinschaft, DFG) under Germany's excellence strategy within the cluster of excellence PhoenixD (EXC 2122, project ID 390833453) and the grant BI 1708/4-1. A.S. and R.T.G. are thankful for financial support from the Hannover School for Nanotechnology (HSN). The authors moreover thank the Laboratory of Nano and Quantum Engineering (LNQE) for providing the TEM facility.

Open Access funding enabled and organized by Projekt DEAL.

Conflict of Interest

The authors declare no conflict of interest.

Data Availability Statement

Research data are not shared.

Keywords

charge carrier separation, gel networks, hybrid nanostructures, metal domain, semiconductor nanoplatelets, semiconductor nanorods

Received: February 9, 2021
Revised: April 30, 2021
Published online: May 29, 2021

[1] F. T. Rabouw, C. de Mello Donega, *Top. Curr. Chem.* **2016**, *374*, 58.
[2] X. Wen, A. Sitt, P. Yu, H. Ko, Y.-R. Toh, J. Tang, *J. Nanopart. Res.* **2012**, *14*, 1278.
[3] X. Wang, J. Yu, R. Chen, *Sci. Rep.* **2018**, *8*, 17323.
[4] D. Dorfs, A. Salant, I. Popov, U. Banin, *Small* **2008**, *4*, 1319.
[5] V. L. Bridewell, R. Alam, C. J. Karwacki, P. V. Kamat, *Chem. Mater.* **2015**, *27*, 5064.
[6] P. Ganguly, M. Harb, Z. Cao, L. Cavallo, A. Breen, S. Dervin, D. D. Dionysiou, S. C. Pillai, *ACS Energy Lett.* **2019**, *4*, 1687.
[7] S. Sanchez-Paradinas, D. Dorfs, S. Friebe, A. Freytag, A. Wolf, N. C. Bigall, *Adv. Mater.* **2015**, *27*, 6152.
[8] D. Zámbó, A. Schlosser, P. Rusch, F. Lübkemann, J. Koch, H. Pfnür, N. C. Bigall, *Small* **2020**, *16*, 1906934.
[9] S. Naskar, J. F. Miethe, S. Sánchez-Paradinas, N. Schmidt, K. Kanthasamy, P. Behrens, H. Pfnür, N. C. Bigall, *Chem. Mater.* **2016**, *28*, 2089.
[10] A. Schlosser, L. C. Meyer, F. Lübkemann, J. F. Miethe, N. C. Bigall, *Phys. Chem. Chem. Phys.* **2019**, *21*, 9002.
[11] J. F. Miethe, F. Luebkemann, A. Schlosser, D. Dorfs, N. C. Bigall, *Langmuir* **2020**, *36*, 4757.
[12] P. Rusch, D. Zámbó, N. C. Bigall, *Acc. Chem. Res.* **2020**, *53*, 2414.
[13] C. She, A. Demortière, E. V. Shevchenko, M. Pelton, *J. Phys. Chem. Lett.* **2011**, *2*, 1469.
[14] Q. Li, K. Wu, J. Chen, Z. Chen, J. R. McBride, T. Lian, *ACS Nano* **2016**, *10*, 3843.
[15] M. D. Tessier, P. Spinicelli, D. Dupont, G. Patriarche, S. Ithurria, B. Dubertret, *Nano Lett.* **2014**, *14*, 207.
[16] P. Kalisman, L. Houben, E. Aronovitch, Y. Kauffmann, M. Bar-Sadan, L. Amirav, *J. Mater. Chem. A* **2015**, *3*, 19679.
[17] T. K. Kormilina, S. A. Cherevkov, A. V. Fedorov, A. V. Baranov, *Small* **2017**, *13*, 1702300.
[18] S. Chen, S. Thota, G. Reggiano, J. Zhao, *J. Mater. Chem. C* **2015**, *3*, 11842.
[19] T. Mokari, *Science* **2004**, *304*, 1787.
[20] L. Carbone, S. Kudera, C. Giannini, G. Ciccarella, R. Cingolani, P. D. Cozzoli, L. Manna, *J. Mater. Chem.* **2006**, *16*, 3952.
[21] G. Menagen, D. Mocatta, A. Salant, I. Popov, D. Dorfs, U. Banin, *Chem. Mater.* **2008**, *20*, 6900.
[22] V. Lesnyak, A. Wolf, A. Dubavik, L. Borchardt, S. V. Voitekhovich, N. Gaponik, S. Kaskel, A. Eychmüller, *J. Am. Chem. Soc.* **2011**, *133*, 13413.
[23] T. Hendel, V. Lesnyak, L. Kühn, A. K. Herrmann, N. C. Bigall, L. Borchardt, S. Kaskel, N. Gaponik, A. Eychmüller, *Adv. Funct. Mater.* **2013**, *23*, 1903.
[24] G. Dukovic, M. G. Merkle, J. H. Nelson, S. M. Hughes, A. P. Alivisatos, *Adv. Mater.* **2008**, *20*, 4306.
[25] P. Rukenstein, A. Teitelboim, M. Volokh, M. Diab, D. Oron, T. Mokari, *J. Phys. Chem. C* **2016**, *120*, 15453.
[26] M. Wächtler, P. Kalisman, L. Amirav, *J. Phys. Chem. C* **2016**, *120*, 24491.
[27] X. Li, J. Lian, M. Lin, Y. Chan, *J. Am. Chem. Soc.* **2011**, *133*, 672.
[28] Y. Nakibli, Y. Mazal, Y. Dubi, M. Wächtler, L. Amirav, *Nano Lett.* **2018**, *18*, 357.
[29] Y. Nakibli, L. Amirav, *Chem. Mater.* **2016**, *28*, 4524.
[30] L. J. Hill, M. M. Bull, Y. Sung, A. G. Simmonds, P. T. Dirlam, N. E. Richey, S. E. DeRosa, I.-B. Shim, D. Guin, P. J. Costanzo, N. Pinna, M.-G. Willinger, W. Vogel, K. Char, J. Pyun, *ACS Nano* **2012**, *6*, 8632.
[31] S. Deka, A. Falqui, G. Bertoni, C. Sangregorio, G. Poneti, G. Morello, M. D. Giorgi, C. Giannini, R. Cingolani, L. Manna, P. D. Cozzoli, *J. Am. Chem. Soc.* **2009**, *131*, 12817.
[32] J. Maynadié, A. Salant, A. Falqui, M. Respaud, E. Shaviv, U. Banin, K. Soulantica, B. Chaudret, *Angew. Chem., Int. Ed.* **2009**, *48*, 1814.
[33] W. Chen, Y. Wang, M. Liu, L. Gao, L. Mao, Z. Fan, W. Shangguan, *Appl. Surf. Sci.* **2018**, *444*, 485.
[34] J. Ran, J. Yu, M. Jaroniec, *Green Chem.* **2011**, *13*, 2708.
[35] Y. Zhang, Z. Jin, X. Yan, H. Wang, G. Wang, *Catal. Lett.* **2019**, *149*, 1174.
[36] Z.-J. Li, X.-B. Fan, X.-B. Li, J.-X. Li, F. Zhan, Y. Tao, X. Zhang, Q.-Y. Kong, N.-J. Zhao, J.-P. Zhang, C. Ye, Y.-J. Gao, X.-Z. Wang,

Q.-Y. Meng, K. Feng, B. Chen, C.-H. Tung, L.-Z. Wu, *J. Mater. Chem. A* **2017**, *5*, 10365.
[37] D. Lang, F. Cheng, Q. Xiang, *Catal. Sci. Technol.* **2016**, *6*, 6207.
[38] S. Naskar, F. Lübkemann, S. Hamid, A. Freytag, A. Wolf, J. Koch, I. Ivanova, H. Pfnür, D. Dorfs, D. W. Bahnemann, N. C. Bigall, *Adv. Funct. Mater.* **2017**, *27*, 1604685.
[39] Y. Nakibli, P. Kalisman, L. Amirav, *J. Phys. Chem. Lett.* **2015**, *6*, 2265.
[40] D. Stone, Y. Ben-Shahar, N. Waiskopf, U. Banin, *ChemCatChem* **2018**, *10*, 5119.
[41] N. Waiskopf, Y. Ben-Shahar, U. Banin, *Adv. Mater.* **2018**, *30*, 1706697.
[42] E. Elmalem, A. E. Saunders, R. Costi, A. Salant, U. Banin, *Adv. Mater.* **2008**, *20*, 4312.
[43] Y. Khalavka, S. Harms, A. Henkel, M. Strozyk, R. Ahijado-Guzmán, C. Sönnichsen, *Langmuir* **2018**, *34*, 187.
[44] L. Carbone, C. Nobile, M. De Giorgi, F. D. Sala, G. Morello, P. Pompa, M. Hytch, E. Snoeck, A. Fiore, I. R. Franchini, M. Nadasan, A. F. Silvestre, L. Chiodo, S. Kudera, R. Cingolani, R. Krahne, L. Manna, *Nano Lett.* **2007**, *7*, 2942.
[45] A. Schlosser, R. T. Graf, N. C. Bigall, *Nanoscale Adv.* **2020**, *2*, 4604.
[46] T. Kodanek, H. M. Banbela, S. Naskar, P. Adel, N. C. Bigall, D. Dorfs, *Nanoscale* **2015**, *7*, 19300.
[47] P. Rusch, B. Schremmer, C. Strelow, A. Mews, D. Dorfs, N. C. Bigall, *J. Phys. Chem. Lett.* **2019**, *10*, 7804.
[48] F. Ren, H. Lu, H. Liu, Z. Wang, Y. Wu, Y. Li, *J. Mater. Chem. A* **2015**, *3*, 23660.
[49] L. Mao, Q. Ba, X. Jia, S. Liu, H. Liu, J. Zhang, X. Li, W. Chen, *RSC Adv.* **2019**, *9*, 1260.
[50] X. Wang, X. Zhang, W. Gao, Y. Sang, Y. Wang, H. Liu, *J. Chem. Phys.* **2020**, *152*, 214701.
[51] Z. Yan, X. Yu, A. Han, P. Xu, P. Du, *J. Phys. Chem. C* **2014**, *118*, 22896.
[52] X. Zhou, J. Jin, X. Zhu, J. Huang, J. Yu, W.-Y. Wong, W.-K. Wong, *J. Mater. Chem. A* **2016**, *4*, 5282.
[53] Y.-C. Liu, J. A. Koza, J. A. Switzer, *Electrochim. Acta* **2014**, *140*, 359.
[54] F. Zhang, Y. J. Liu, Q. H. Liu, Q. Li, H. Li, X. Y. Cai, Y. D. Wang, *Mater. Technol.* **2013**, *28*, 310.
[55] B. Xia, I. W. Lenggoro, K. Okuyama, *J. Mater. Sci.* **2001**, *36*, 1701.
[56] A.-G. Boudjahem, S. Monteverdi, M. Mercy, M. M. Bettahar, *Langmuir* **2003**, *20*, 208.
[57] T. Matsumoto, K. Takahashi, K. Kitagishi, K. Shinoda, J. L. Cuya Huaman, J.-Y. Piquemal, B. Jeyadevan, *New J. Chem.* **2015**, *39*, 5008.
[58] B. Jung, W. Deng, Y. Li, B. Batchelor, A. Abdel-Wahab, *Environ. Sci. Eur.* **2020**, *32*, 8.
[59] M. Abdellah, S. Zhang, M. Wang, L. Hammarström, *ACS Energy Lett.* **2017**, *2*, 2576.
[60] Y. Ben-Shahar, J. P. Philbin, F. Scotognella, L. Ganzer, G. Cerullo, E. Rabani, U. Banin, *Nano Lett.* **2018**, *18*, 5211.
[61] A. Hinsch, S.-H. Lohmann, C. Strelow, T. Kipp, C. Würth, D. Geißler, A. Kornowski, C. Wolter, H. Weller, U. Resch-Genger, A. Mews, *J. Phys. Chem. C* **2019**, *123*, 24338.
[62] J. J. Li, Y. A. Wang, W. Guo, J. C. Keay, T. D. Mishima, M. B. Johnson, X. Peng, *J. Am. Chem. Soc.* **2003**, *125*, 12567.
[63] Y. Liu, P. Stradins, S.-H. Wei, *Sci. Adv.* **2016**, *2*, e1600069.